Key Points:
- Development of a bowtie technique for the calibration of the GOES-R satellite series SEISS MPS-HI electron data
- Cross-satellite comparison of the electron data sets from various GOES satellites
- Comparison of the >2-MeV electron channel (used for space weather alerts by SWPC) with the analogous channel from older instruments

Correspondence to:
A. Boudouridis,
athanasios.boudouridis@noaa.gov

Development of a Bowtie Inversion Technique for Real-Time Processing of the GOES-16/-17 SEISS MPS-HI Electron Channels

A. Boudouridis[1,2] , J.V. Rodriguez[1,2] , B.T. Kress[1,2], B.K. Dichter[3], and T.G. Onsager[4]

[1]Cooperative Institute for Research in Environmental Sciences, University of Colorado, Boulder, CO, USA, [2]National Center for Environmental Information, National Oceanic and Atmospheric Administration, Boulder, CO, USA, [3]Assurance Technology Corporation, Carlisle, MA, USA, [4]Space Weather Prediction Center, National Oceanic and Atmospheric Administration, Boulder, CO, USA

Abstract The Space Environment In-Situ Suite on the Geostationary Operational Environmental Satellite (GOES)-R series of satellites includes a new instrument for measuring radiation belt electrons and protons, the Magnetospheric Particle Sensor–High Energy (MPS-HI). The MPS-HI electron channels cover the energy range 50 keV to 4 MeV. The conversion of raw MPS-HI electron telescope counts to fluxes is based on the so-called bowtie technique. The goal of the bowtie analysis is to calculate for each energy channel an energy/geometric factor pair applicable to a wide range of energy spectra and for which the geometric factor error is minimized. Rather than using idealized analytical spectral functions, we use observed high-resolution spectra from the cross-calibrated Combined Release and Radiation Effects Satellite (CRRES) Medium Electron Sensor A and High Energy Electron Fluxmeter data set from the period 1990–1991, restricted to $6 < L < 8$. One thousand randomly selected CRRES spectra are used to perform the bowtie analysis and determine the MPS-HI channel energy/geometric factor characteristics. The results are used to convert the GOES-16/-17 MPS-HI electron counts to fluxes. The same bowtie technique is used to calculate effective energies and geometric factors for the GOES-13/-14 Magnetospheric Electron Detector ME1-ME5 (30–600 keV) electron channels. We compare the fluxes from the various spacecraft (GOES-16/-13, GOES-17/-14, and GOES-16/-17) over periods of several months to determine the applicability and utility of the bowtie analysis. Finally, we compare the GOES-16/-13 fluxes during 22 days of near conjunction. All comparisons show good agreement among the various satellite data sets.

1. Introduction

The ability of energetic electrons in the outer radiation belt to penetrate satellite shielding with deleterious effects was recognized in the specification of the original Space Environment Monitor (SEM) flown on the two Synchronous Meteorological Satellites and the first Geostationary Operational Environmental Satellite (GOES) (Grubb, 1975) launched, respectively, in 1974, 1975, and 1975. The SEM channel set included an electron channel with a lower energy bound of 2 MeV in order to characterize the source of background counts in the X-ray sensor. "The single electron channel was intended primarily to provide an independent monitor of the electron environment critical to the X-ray sensor performance, and the threshold of this channel was adjusted to match the expected sensitivity of the X-ray instrument" (Grubb, 1975, p. 4-1). Within a few years, the GOES MeV electron data were being used for scientific studies of the dynamics of >2 MeV electron fluxes during substorms (Nagai, 1982), as well as to correlate the radiation environment with anomalies on other satellites. Certain anomalies were attributed to energetic electrons that lodged in dielectrics after penetrating shielding, leading to discharges that radiated electromagnetic pulses, causing spurious commands (Vampola, 1987). Continued accumulation of evidence of a correlation between >2-MeV electron fluxes and satellite anomalies (e. g., Wrenn, 1995; Wrenn & Smith, 1996) led to the creation of the National Oceanic and Atmospheric Administration (NOAA) real-time >2-MeV electron flux alert, first issued on 18 May 1995. This alert is issued by the Space Weather Prediction Center when the 5-min averaged GOES >2-MeV flux exceeds 1,000 electrons/(cm^2·sr·s).

In order to improve the real-time observation of electron fluxes that cause internal charging, the original electron channel (> 1.25 or >2 MeV, depending on the satellite) was augmented on GOES-8 (launched 1994) with two additional integral channels (>0.8 and >4 MeV) (Onsager et al., 1996). Starting with
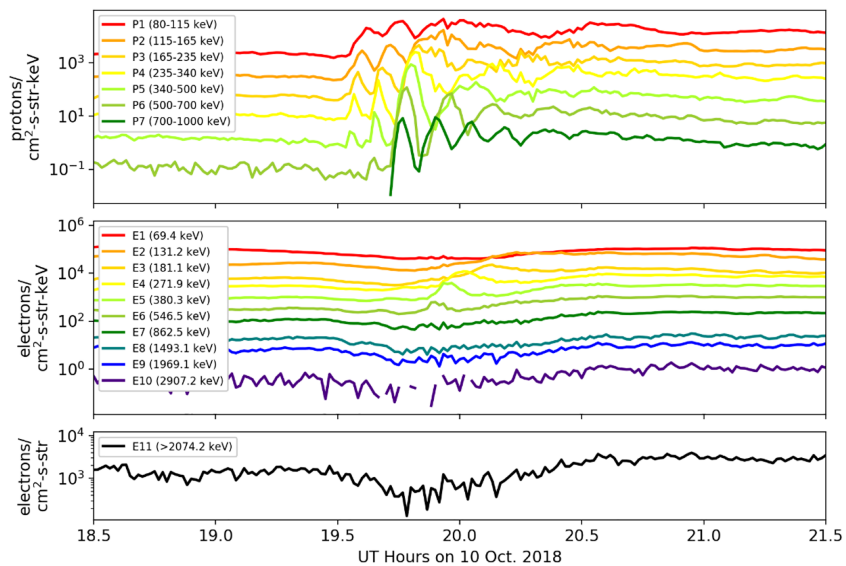
Figure 1. Examples of GOES-16 MPS-HI Level-1b data showing proton (upper panel) and electron (lower two panels) injections from the magnetotail during 1830–2130 UT on 10 October 2018. The time series shown are from proton telescope 2 and electron telescope 4. Telescopes 2 and 4 are the central proton and electron telescopes, respectively, looking radially outward in the orbital (geographic equatorial) plane, nominally directed perpendicular to the magnetic field direction. The proton energy channel bounds given in the legend are the nominal Full Widths at Half Maximum points of the proton channel response functions. The electron energies given are effective energies for telescope 4, derived using the bowtie method as described in this paper. Proton channels P8–P11 have significant counts above background only during solar proton events, thus are not shown.

GOES-13, a Magnetospheric Electron Detector (MAGED) was added to the SEM suite that measured 30 to 600-keV electrons (Hanser, 2011; Rowland & Weigel, 2012). MAGED was based on the Medium Energy Proton and Electron Detector electron telescopes first flown on TIROS-N in 1978. For the GOES-R series, rather than continuing the use of designs from the 1970s, a new instrument was designed to observe electron fluxes at energies that contribute to internal charging (> 100 keV) (National Aeronautics and Space Administration, 2011).

The GOES-R satellites are the newest GOES spacecraft operated by NOAA. Two of these satellites, GOES-16 and GOES-17, are already in orbit, with two more to be launched in the near future. GOES-16 was launched on 19 November 2016 and GOES-17 on 1 March 2018. Both spacecraft carry the Space Environment In-Situ Suite (SEISS), a collection of four instruments tasked with measuring the energetic particle environment at geostationary orbit.

One of the four instruments is the Magnetospheric Particle Sensor–High Energy (MPS-HI), a new instrument designed to measure radiation belt electrons and protons (Dichter et al., 2015). It is comprised of five electron and five proton telescopes, each with a 30° full-width conical field of view (FOV). The telescopes for each species are arranged from north to south at five look directions with FOV centers separated by 35°, with the central telescope viewing in the zenith (anti-earthward) direction. Each electron telescope measures electrons in 10 differential channels, logarithmically spaced in the energy range 50 keV to 4 MeV, and two integral channels at energies >2 and >4.3 MeV. Each proton telescope measures protons in 11 differential logarithmic channels that cover the energy range from 80 keV to 12 MeV. The cadence for the electron and proton measurements is 1 s.

Figure 1 shows examples of GOES-16 MPS-HI proton (upper panel) and electron (lower two panels) data during 1830–2130 UT on 10 October 2018. The proton and electron time series show signatures of proton and electron injections from the magnetotail. The injections are characterized by a sudden increase in flux level, with higher energies arriving at the spacecraft location first followed by subsequent "drift echoes," as the injected protons and electrons drift around the Earth and repeatedly reappear at the spacecraft location. The 5-min averaged Level-1b electron fluxes shown are processed from Level-0 count rates using the inversion method described in this paper.

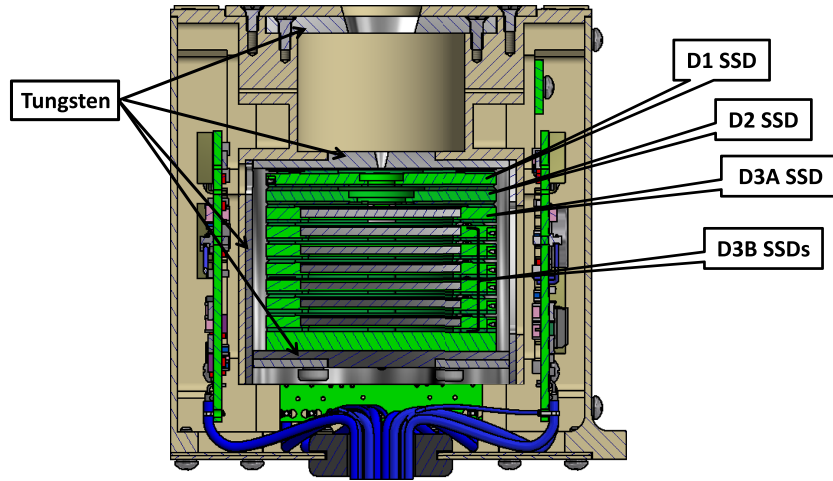SEISS-MA-7020, ASSEMBLY, ELECTRON TELESCOPE, MPS-HI,
SECTION VIEW

Figure 2. A cross-section of the MPS-HI electron telescope assembly showing the arrangement of the solid state detectors (SSDs).

In this paper, we discuss the calibration of the 10 differential electron channels plus the >2-MeV integral electron channel used by GOES-16/-17. The accurate calibration of these channels is essential for the utility of these data, both for scientific studies as well as for the continuity of space weather alerts. In addition, as these and other satellite measurements are increasingly used in global data assimilative models, it will be necessary to ensure accurate intercalibration of data among multiple satellites and to be able to map the electron data reliably to locations throughout the magnetosphere. A cross-section of the electron telescope assembly, showing the arrangement of the solid state detectors (SSDs), is shown for reference in Figure 2.

2. Inversion of MPS-HI Raw Electron Data

The instrument measured quantity is the count rate R in counts per second. This relates to the physical quantity, flux $j(E)$ in counts/(s·cm^2·sr·keV), through the convolution of $j(E)$ with the geometric factor $G(E)$ (GF or channel response function, in cm^2·sr) of the specific channel according to the equation

$$R = \int_0^\infty j(E)G(E)dE, \tag{1}$$

where E is the particle energy and the integration is over all energies. The GF for each channel is derived by integrating channel effective area over solid angle assuming isotropic flux over the FOV. The channel effective area is measured in an electron beam and simulated using the GEometry ANd Tracking (GEANT4) model, a numerical simulation of the passage of particles through matter (in our case, the solid state detectors of the instrument). The GFs used in the analysis for this paper were constructed from a combination of beam measurements and GEANT4 simulations using B-spline fits (Dierckx, 1993). For a detailed description, see Appendix A. The challenge is to unfold $j(E)$ from observations using characterization of broad energy channels, often including long high-energy tails.

2.1. The Bowtie Inversion Technique

The purpose of the bowtie analysis is to identify a GF, effective energy/energy threshold pair (for a differential/integral channel, respectively), that is applicable to a wide range of energy spectra and for which the GF error is minimized (Fillius & McIlwain, 1974; Selesnick & Blake, 2000; Van Allen et al., 1974). This approach enables a reasonably accurate yet simple conversion of channel count rates to differential/integral flux. A family of curves in [G,E] space is generated from the following integrals of representative electron
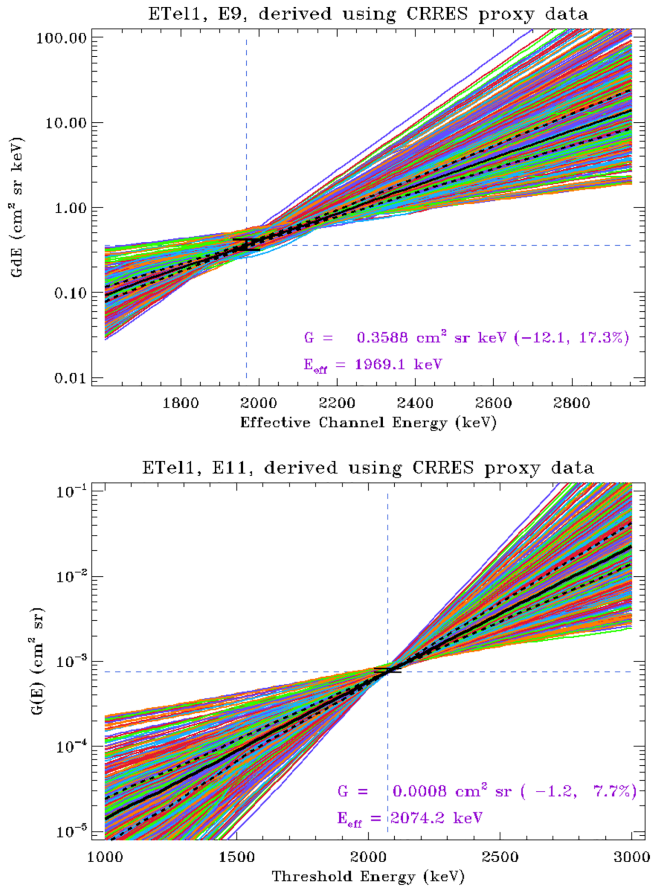
Figure 3. Bowtie [G,E] plots for the GOES-16 MPS-HI telescope 1 (ETel1) channels E9 (differential, top) and E11 (integral, bottom). The multicolor curves, derived from equations 2 and 3, correspond to the 1,000 randomly selected CRRES spectra. The solid black curve is the median of the distribution, and the dashed black curves above and below are the 75th and 25th percentiles, respectively.

Figure 4. One thousand randomly selected CRRES spectra used to train the bowtie analysis. The solid black curve is the median of the distribution, and the dashed black curves above and below are the 75th and 25th percentiles, respectively.
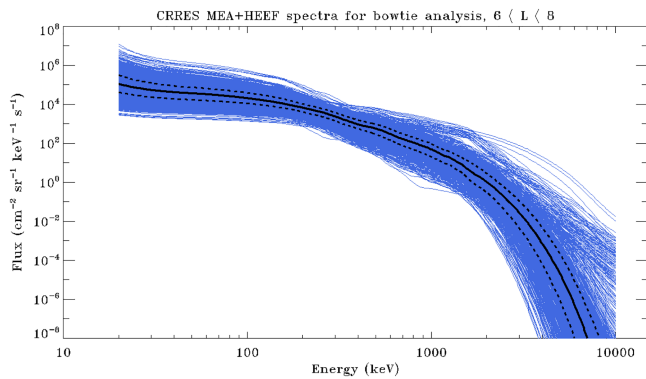
flux spectra for a range of candidate effective energies, E_{eff}, for a differential channel (equation 2), or energy thresholds, E_T, for an integral channel (equation 3):

$$GdE = \frac{\int_0^\infty j(E)G(E)dE}{j(E_{\text{eff}})}, \tag{2}$$

$$G_I = \frac{\int_0^\infty j(E)G(E)dE}{\int_{E_T}^\infty j(E)dE}, \tag{3}$$

where $j(E_{\text{eff}})$ is the representative electron flux spectrum value at the candidate E_{eff}.

The name "bowtie" is derived from the form of the family of curves in the [G,E] plot, the bowtie (see Figure 3 below). The solution lies at the "knot" in the bowtie: the tighter the "knot", the better the solution. (This is not the same as a B-spline knot.) A nonlinear minimization technique (Nelder & Mead, 1965) is used to find the knot location and determine its effective energy value. The minimized function is the difference between the 5th and 95th percentiles of the GF distribution at a given energy, normalized to the median GF. From the initial guess energy, two searches are performed, one starting to step down in energy and one starting to step upwards. If they agree to within a tolerance, the results of the two searches are averaged and reported as the effective energy. The median, 5th, and 95th percentiles of GdE or G are determined for this energy.

For a differential electron channel, the flux $j(E)$ is attributed to the bowtie effective energy related to the bowtie GF quantity, GdE, through the equation

$$j(E_{\text{eff}}) = {}^R/_{GdE}, \tag{4}$$

where R is the measured quantity given by (1). For an integral channel, the flux for energies higher than the bowtie threshold energy, E_T, is given by the relation

$$j(E > E_T) = {}^R/_{GI}, \tag{5}$$

where G_I is the bowtie GF and R is given by (1).

2.2. The CRRES Proxy Data Set

The application of the bowtie technique requires a proxy data set on which to "train" the bowtie analysis, meaning use of a variety of possible spectra to derive the [G,E] pair for each electron energy channel. Past studies have exclusively used analytical spectra, such as power-law spectra, $j(E) = E^{-\gamma}$, or exponential spectra, $j(E) = e^{-qE}$. However, a bowtie analysis using a range of analytical forms without consideration of the natural distribution of such spectra leaves open the question of how representative the results are. Recently, to address this question, Sandberg et al. (2019) performed a bowtie analysis of the energy responses of the Galileo Environmental Monitoring Units using a representative distribution of power law and exponential fits to Van Allen Probes observations. In the present paper, an extensive data set of observed energetic electron flux spectra is used to train the bowtie analysis. In the following, we describe the methodology behind the use of the cross-calibrated Combined

Table 1
Bowtie Parameters for the GOES-16 MPS-HI Electron Telescopes (GdE in $cm^2 \cdot sr \cdot keV$, and G in $cm^2 \cdot sr$)

GOES-16	ETel1				ETel2				ETel3			
Channel	Eb (keV)	GdE(5%)	GdE(50%)	GdE(95%)	Eb (keV)	GdE(5%)	GdE(50%)	GdE(95%)	Eb (keV)	GdE(5%)	GdE(50%)	GdE(95%)
E1S	76.2	3.84E-02	3.88E-02	3.94E-02	70.9	3.91E-02	3.95E-02	4.02E-02	56.3	4.30E-02	4.34E-02	4.44E-02
E2	131.2	5.77E-02	6.03E-02	7.05E-02	131.2	5.77E-02	6.03E-02	7.05E-02	131.2	5.77E-02	6.03E-02	7.05E-02
E3t	181.0	7.13E-02	7.67E-02	8.55E-02	178.9	6.67E-02	7.09E-02	7.84E-02	186.0	6.96E-02	7.82E-02	9.08E-02
E4	271.9	7.49E-02	8.47E-02	9.84E-02	271.9	7.49E-02	8.47E-02	9.84E-02	319.0	1.22E-01	1.34E-01	1.50E-01
E5	380.3	1.67E-01	1.79E-01	1.96E-01	380.3	1.67E-01	1.79E-01	1.96E-01	445.0	2.30E-01	2.56E-01	2.87E-01
E6	546.5	2.83E-01	3.01E-01	3.21E-01	546.5	2.83E-01	3.01E-01	3.21E-01	677.5	2.59E-01	2.72E-01	2.91E-01
E7	905.8	5.38E-01	5.73E-01	6.31E-01	862.5	4.53E-01	4.83E-01	5.33E-01	931.2	5.13E-01	5.43E-01	5.97E-01
E8	1493.1	2.14E-01	2.45E-01	2.96E-01	1493.1	2.14E-01	2.45E-01	2.96E-01	1493.1	2.14E-01	2.45E-01	2.96E-01
E9	1969.1	3.15E-01	3.59E-01	4.21E-01	1969.1	3.15E-01	3.59E-01	4.21E-01	1969.1	3.15E-01	3.59E-01	4.21E-01
E10	2907.2	5.92E-01	6.04E-01	7.86E-01	2907.2	5.92E-01	6.04E-01	7.86E-01	2907.2	5.92E-01	6.04E-01	7.86E-01
	Et (keV)	G (5%)	G (50%)	G (95%)	Et (keV)	G (5%)	G (50%)	G (95%)	Et (keV)	G (5%)	G (50%)	G (95%)
E11	2074.2	7.46E-04	7.55E-04	8.13E-04	2074.2	7.46E-04	7.55E-04	8.13E-04	2074.2	7.46E-04	7.55E-04	8.13E-04

GOES-16	ETel4				Etel5			
Channel	Eb (keV)	GdE(5%)	GdE(50%)	GdE(95%)	Eb (keV)	GdE(5%)	GdE(50%)	GdE(95%)
E1S	69.4	4.16E-02	4.19E-02	4.27E-02	65.5	4.87E-02	4.90E-02	4.98E-02
E2	131.2	5.43E-02	5.67E-02	6.63E-02	131.2	5.77E-02	6.03E-02	7.05E-02
E3t	181.1	5.97E-02	6.53E-02	7.43E-02	191.0	8.13E-02	9.07E-02	1.05E-01
E4	271.9	7.05E-02	7.97E-02	9.26E-02	308.0	1.36E-01	1.50E-01	1.71E-01
E5	380.3	1.57E-01	1.68E-01	1.84E-01	478.0	2.40E-01	2.54E-01	2.71E-01
E6	546.5	2.66E-01	2.83E-01	3.02E-01	684.2	2.79E-01	2.91E-01	3.15E-01
E7	862.5	4.26E-01	4.55E-01	5.01E-01	939.2	4.66E-01	4.93E-01	5.44E-01
E8	1493.1	2.01E-01	2.30E-01	2.79E-01	1493.1	2.14E-01	2.45E-01	2.96E-01
E9	1969.1	2.97E-01	3.38E-01	3.96E-01	1969.1	3.15E-01	3.59E-01	4.21E-01
E10	2907.2	5.92E-01	6.04E-01	7.86E-01	2907.2	5.92E-01	6.04E-01	7.86E-01
	Et (keV)	G (5%)	G (50%)	G (95%)	Et (keV)	G (5%)	G (50%)	G (95%)
E11	2074.2	7.46E-04	7.55E-04	8.13E-04	2074.2	7.46E-04	7.55E-04	8.13E-04

Release and Radiation Effects Satellite (CRRES) spacecraft Medium Electron Sensor A (MEA) and High Energy Electron Fluxmeter (HEEF) instruments data set (Johnston et al., 2014).

CRRES was in a geosynchronous transfer orbit and returned data from July 1990 to October 1991. The MEA instrument measured energetic electrons between 148 keV and 1.582 MeV in 17 differential energy channels with resolution higher than MPS-HI. It was considered the "gold standard" for energetic electron observations prior to the launch of the Van Allen Probes. The HEEF instrument provides electron observations in the range 0.65–7.5 MeV in 11 differential energy channels. Both instruments return pitch-angle resolved measurements, but omnidirectional fluxes are used in this study.

In order to create a proxy data set appropriate for the training of the bowtie analysis to be used in the calibration of the GOES MPS-HI instrument, the following steps are taken:

1. Only observations within the spatial range $6 \leq L < 8$ are used, where L is the L-shell parameter. This range of L corresponds to that of geostationary orbit under a realistic range of geomagnetic conditions (Baker et al., 2019), $L = 6.6$ being the value in a dipole field.
2. Times when simultaneous MEA and HEEF data are present are selected.
3. Only spectra for which the fluxes at the MEA 1.582-MeV channel and the HEEF 1.6-MeV channel agree within a factor of 2 are kept.
4. MEA fluxes are used up to energy 1.472 MeV, plus the average of the MEA 1.582-MeV and HEEF 1.6-MeV channel fluxes.

Table 2
Bowtie Parameters for the GOES-17 MPS-HI Electron Telescopes (GdE in $cm^2 \cdot sr \cdot keV$, and G in $cm^2 \cdot sr$)

GOES-17	ETel1				ETel2				ETel3			
Channel	Eb (keV)	GdE(5%)	GdE(50%)	GdE(95%)	Eb (keV)	GdE(5%)	GdE(50%)	GdE(95%)	Eb (keV)	GdE(5%)	GdE(50%)	GdE(95%)
E1S	73.2	5.50E-02	5.54E-02	5.68E-02	73.1	4.80E-02	4.84E-02	4.97E-02	74.1	5.16E-02	5.20E-02	5.34E-02
E2	128.2	8.70E-02	8.91E-02	9.87E-02	129.2	7.10E-02	7.32E-02	8.26E-02	130.2	6.11E-02	6.35E-02	7.36E-02
E3t	180.7	7.27E-02	7.86E-02	8.96E-02	180.7	6.88E-02	7.45E-02	8.49E-02	180.7	6.57E-02	7.11E-02	8.11E-02
E4	277.9	9.16E-02	1.03E-01	1.19E-01	277.9	8.67E-02	9.76E-02	1.13E-01	277.9	8.28E-02	9.32E-02	1.08E-01
E5	378.5	1.86E-01	2.00E-01	2.19E-01	378.5	1.77E-01	1.90E-01	2.07E-01	378.5	1.69E-01	1.81E-01	1.98E-01
E6	547.0	3.22E-01	3.42E-01	3.65E-01	547.0	3.04E-01	3.24E-01	3.46E-01	546.9	2.91E-01	3.09E-01	3.30E-01
E7	864.7	5.18E-01	5.54E-01	6.09E-01	864.7	4.90E-01	5.24E-01	5.77E-01	864.7	4.68E-01	5.01E-01	5.51E-01
E8	1493.1	2.46E-01	2.81E-01	3.41E-01	1493.8	2.34E-01	2.67E-01	3.24E-01	1493.1	2.23E-01	2.54E-01	3.08E-01
E9	1969.5	3.56E-01	4.05E-01	4.75E-01	1969.5	3.37E-01	3.84E-01	4.50E-01	1969.5	3.22E-01	3.67E-01	4.30E-01
E10	2893.8	6.35E-01	6.47E-01	8.55E-01	2893.8	6.02E-01	6.12E-01	8.10E-01	2893.8	5.74E-01	5.85E-01	7.73E-01
	Et (keV)	G (5%)	G (50%)	G (95%)	Et (keV)	G (5%)	G (50%)	G (95%)	Et (keV)	G (5%)	G (50%)	G (95%)
E11	2074.8	8.41E-04	8.51E-04	9.17E-04	2074.8	7.96E-04	8.06E-04	8.69E-04	2074.8	7.60E-04	7.70E-04	8.29E-04

GOES-17	ETel4				Etel5			
Channel	Eb (keV)	GdE(5%)	GdE(50%)	GdE(95%)	Eb (keV)	GdE(5%)	GdE(50%)	GdE(95%)
E1S	75.0	4.72E-02	4.75E-02	4.88E-02	71.1	5.03E-02	5.07E-02	5.21E-02
E2	131.0	5.97E-02	6.25E-02	7.41E-02	129.1	8.36E-02	8.70E-02	9.39E-02
E3t	180.7	7.04E-02	7.62E-02	8.68E-02	180.7	6.78E-02	7.34E-02	8.37E-02
E4	277.9	8.87E-02	9.99E-02	1.15E-01	277.9	8.55E-02	9.62E-02	1.11E-01
E5	378.5	1.81E-01	1.94E-01	2.12E-01	378.5	1.74E-01	1.87E-01	2.04E-01
E6	547.0	3.12E-01	3.31E-01	3.54E-01	546.9	3.00E-01	3.19E-01	3.41E-01
E7	864.7	5.02E-01	5.36E-01	5.90E-01	864.7	4.83E-01	5.17E-01	5.68E-01
E8	1493.1	2.39E-01	2.73E-01	3.30E-01	1493.1	2.30E-01	2.63E-01	3.18E-01
E9	1969.5	3.45E-01	3.93E-01	4.60E-01	1969.5	3.33E-01	3.78E-01	4.44E-01
E10	2893.8	6.15E-01	6.26E-01	8.29E-01	2893.8	5.93E-01	6.03E-01	7.98E-01
	Et (keV)	G (5%)	G (50%)	G (95%)	Et (keV)	G (5%)	G (50%)	G (95%)
E11	2074.8	8.15E-04	8.25E-04	8.89E-04	2074.8	7.85E-04	7.95E-04	8.56E-04

5. HEEF spectra>1.6 MeV are fitted to exponentials or power laws depending on counting statistics and lack or presence of good quality data, respectively. Details of this process are provided in Appendix B.
6. Extrapolation is performed down to 20 keV by fitting exponentials to the lowest-energy MEA channels in order to cover the MPS-HI lowest-energy channel.

The resulting proxy data set contains 79,979 CRRES spectra conforming to the above requirements. One thousand of these spectra are randomly selected to train the bowtie analysis and produce the channel GFs and effective energies. Figure 4 shows the CRRES spectra used for the training of the bowtie procedure. The bowtie $[GdE, E_{\text{eff}}]$ and $[G_I, E_T]$ plots for the GOES-16 MPS-HI telescope 1 (ETel1) channels E9 (differential, top) and E11 (integral, bottom), respectively, are shown in Figure 3. The resulting bowtie quantities are denoted on the plots. The percentages in the parentheses next to the mean GF indicate the percent fractional difference of the mean value (50%) from the 5th and 95th percentiles used in the minimization technique that determines the channel effective energy. These are the errors of the reported GFs.

The ability of the bowtie technique to accurately produce particle fluxes can be demonstrated using the already known CRRES fluxes. Equation 1 provides the count rates that would have been observed in an energy channel given the $G(E)$ response of that channel and a proxy CRRES flux $j(E)$, both interpolated on a logarithmically spaced interval from 20 keV to 10 MeV. This is known as the forward model that provides the count rate for a known flux. Using the bowtie parameters derived for that channel through the use of the 1,000 random proxy CRRES spectra, we can then derive the expected CRRES flux for this energy channel through equations 4 or 5. This is the inverted model that yields the flux for a known count rate. This

Table 3

Calibration Parameters for the GOES-13/-14 MAGED Electron Telescopes. Columns 5 and 6 are the Results of the Bowtie Analysis, Columns 3 and 4 are the Originally Used Energies and Geometry-Energy Factors (Hanser, 2011)

MAGED	Original			Bowtie		
Channel	Bandpass (keV)	Ec (keV)	*GdE* (cm^2·sr·keV)	Eb (keV)	*GdE* (cm^2·sr·keV)	(50%)
ME1	30–50	40	0.2	68.3	0.341	
ME2	50–100	75	0.5	91.3	0.643	
ME3	100–200	150	1.0	176.6	1.844	
ME4	200–350	275	1.5	264.1	2.012	
ME5	350–600	475	2.5	493.9	3.162	

process is applied to the remaining 78,979 proxy CRRES spectra (barring the training spectra to avoid contamination of the estimated errors below). The retrieved fluxes are then compared to the true fluxes by estimating their fractional error and making error histograms for each channel. The results were tested using GOES-16 MPS-HI electron telescope 1. The average and standard deviation of the error histogram are calculated for each channel. The average error of the CRRES flux reproduction is always within a few percentage points from 0, while the standard deviation rarely exceeds 10%. Considering the very large CRRES spectra sample, these results clearly demonstrate the accuracy of the bowtie technique and justify its use for the GOES-16/-17 MPS-HI electron channels.

3. Application to the GOES Satellites

The bowtie parameters derived for the MPS-HI channels through the CRRES proxy data set can then be applied to the GOES-R data sets. Separate bowtie parameter sets are produced for each of the GOES-16 and GOES-17 telescopes because the MPS-HI telescopes are all individually calibrated. Tables 1 and 2 provide the results of the bowtie analysis for all telescopes, GOES-16 and -17, respectively.

Similarly, identical bowtie analyses are performed for the MAGED instrument onboard the GOES-13 and GOES-14 spacecraft. The MAGED instrument has nine telescopes (look directions), each with 30° full cone angle. Five are arranged in a North-South fan, and four more form an East-West fan, with the central telescope directed radially anti-earthward. Each telescope measures energetic electrons in five energy channels in nominal energy ranges, 30–50, 50–100, 100–200, 200–350, and 350–600 keV. Bowtie plots, like the ones of Figure 3, yield the bowtie [*G,E*] pairs for all these telescopes and energy channels. Table 3 summarizes the bowtie results for the MAGED instruments, with columns 3 and 4 providing the originally used channel midpoint energies and geometry-energy factors (cm^2·sr·keV) for comparison. The design values of the GFs and channel energy ranges, confirmed by beam calibrations of a single MAGED telescope (Panametrics, 2004), are used in the NOAA processing of all MAGED telescopes to convert counts to fluxes (Hanser, 2011). (In contrast, the MPS-HI telescopes were individually calibrated.) The Space Weather Prediction Center processing converts the MAGED counts to differential flux by dividing by the geometry-energy factors. Therefore, the bowtie results were used to scale the publicly available MAGED fluxes by multiplying them by the ratio of the original geometry-energy factors to the bowtie geometry-energy factors and by assigning them to the bowtie effective energy for comparison with GOES-16 and GOES-17 fluxes.

In the following sections, we perform cross-satellite comparisons of 1-min average spectra distributions, all produced with the bowtie technique, between telescopes of the same orientation on the various GOES satellites. Table 4 identifies the telescopes on the four satellites that are at the same orientation relative to the orbital plane during these periods and therefore can be compared directly. (The satellites can operate in both the upright and inverted state and transition from one to the other via a rotation about the spacecraft yaw axis.) Apart from the near-conjunction case, the pairs of satellites were separated by approximately 1 hr in local time. Cross-calibrations of GOES >2-MeV fluxes have demonstrated that such a small separation, when geostationary satellites are nearly at the same geomagnetic latitude, enables accurate comparisons (Meredith et al., 2015; Onsager et al., 2004).

3.1. GOES-16 and GOES-13 Cross-Satellite Comparison

Figure 5 shows the results of an asynchronous statistical comparison of electron fluxes from two spacecraft/instruments, GOES-16 MPS-HI and GOES-13 MAGED, as spectra of electron flux percentiles. The comparison is between telescopes with the same orientation, telescope 1 of MPS-HI and telescope 6 of MAGED, both looking at 35° north of the equatorial plane. The period of comparison is from 9 January 2017 to 31 October

Table 4

Orientation Relative to the Orbital Plane of the MAGED and MPS-HI Electron Telescopes on GOES-13, GOES-14, GOES-16, and GOES-17 During the Periods Used for Cross-Calibration in This Paper

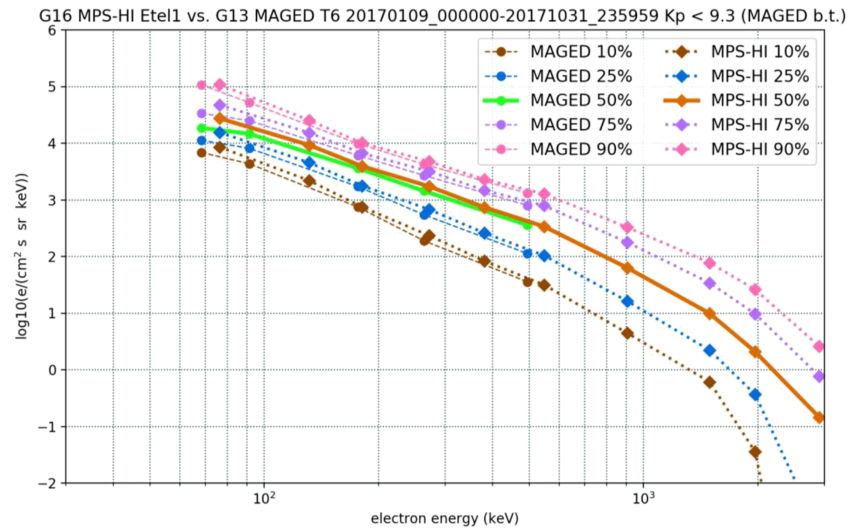|	Electron telescope number			
Orientation	GOES-13 (upright)	GOES-14 (inverted)	GOES-16 (upright)	GOES-17 (upright)
70°N	9	7	3	3
35°N	6	8	1	1
0°	1	1	4	4
35°S	8	6	2	2
70°S	7	9	5	5

Figure 5. Comparison of GOES-16 MPS-HI telescope 1 and GOES-13 MAGED telescope 6 1-min percentile spectra. The period of comparison is 9 January 2017 to 31 October 2017.

2017, when both spacecraft were transmitting data and separated by approximately an hour in local time (GOES-16 at 89.5°W and GOES-13 at 75°W). Flux percentiles for the five MAGED channels and the 10 MPS-HI differential electron channels are plotted at the bowtie effective energies. Diamonds indicate MPS-HI data and circles MAGED data. The solid curves denote the median spectrum (50th percentile), orange for MPS-HI and green for MAGED. The remaining curves correspond to higher or lower percentiles. There is very good agreement between the two distributions, with a small deviation at the lowest MAGED channel. The comparisons for the five pairs of MAGED and MPS-HI telescopes that look in the same direction are summarized in Table 5. The comparisons are made by taking the ratio of the GOES-13 to the GOES-16 percentile fluxes, following interpolation to five common energies (80, 130, 180, 270, and 380 keV) assuming a piecewise power-law distribution. These energies were chosen so that no extrapolation was required.

3.2. GOES-16 and GOES-13 Near-Conjunction Period

Following a station change, GOES-16 reached the GOES-east longitude (75.2°W) on 11 December 2017, and GOES-13 was moved to 74.5°W. For the following 22 days, until 2 January 2018 (when the GOES-13 particle data ceased to flow), it was possible to compare GOES-16 MPS-HI and GOES-13 MAGED in near conjunction. Figure 6 shows time series during this period from MPS-HI telescope 3 and MAGED telescope 9, both looking 70° north of the equatorial plane. The time series from the two satellites exhibit similar fine structure, including injections, drift echoes, and dropouts, reflecting the high quality of both sets of measurements. Figure 7 shows the percentile spectra from this near-conjunction period, and Table 6 tabulates the percentile comparisons for all five telescope pairs, both in the same format as in the previous section. (The 15-hr period of missing GOES-16 data on 18 December 2017 was omitted from the statistical comparison.)

3.3. GOES-17 and GOES-14 Cross-Satellite Comparison

Figure 8 shows spectra of electron flux percentiles from GOES-17 MPS-HI telescope 1 and GOES-14 MAGED telescope 8, again with the same look directions. The period of comparison in this case is 20 June 2018 to 24 September 2018. (GOES-14 was inverted during this period, resulting in the order of the MAGED telescopes being inverted.) During this period, GOES-17 was at 89.5°W and GOES-14 was at 105°W. The plot format is the same as in Figure 5, and all five telescope pair comparisons are summarized in Table 7, as before. As with the previous spacecraft pair, the two distributions follow each other very closely, with small exceptions at the lowest and highest MAGED channels.

Table 5
Comparisons for the Five Pairs of GOES-13 MAGED and GOES-16 MPS-HI Telescopes That Look in the Same Direction. The Values are the Ratio of the GOES-13 to the GOES-16 Percentile Fluxes Interpolated at Five Energies

| E (keV)	MT9 : ET3					MT6 : ET1					MT1 : ET4					MT8 : ET2					MT7 : ET5			
	10	25	50 (Q)	75	90	10	25	50 (Q)	75	90	10	25	50 (Q)	75	90	10	25	50 (Q)	75	90	25	50 (Q)	75	90
80	1.08	1.01	0.98	1.00	1.05	0.71	0.68	0.66	0.66	0.76	0.77	0.73	0.70	0.70	0.78	0.81	0.74	0.73	0.75	0.82	0.77	0.78	0.81	0.95
130	1.15	1.11	1.09	1.10	1.20	0.75	0.76	0.73	0.75	0.82	0.74	0.70	0.67	0.68	0.76	0.70	1.00	0.99	1.00	1.04	0.69	0.71	0.75	0.81
180	0.93	0.90	0.88	0.90	0.93	0.91	0.90	0.86	0.86	0.92	1.44	1.33	1.25	1.25	1.33	0.71	0.96	0.97	0.98	0.99	0.68	0.69	0.73	0.78
270	0.77	0.78	0.81	0.83	0.85	0.74	0.74	0.78	0.80	0.84	0.72	0.72	0.73	0.75	0.76	0.74	1.00	1.03	1.06	1.09	0.75	0.77	0.81	0.84
380	0.91	0.89	0.89	0.91	0.94	0.86	0.83	0.87	0.90	0.93	0.84	0.79	0.81	0.84	0.86	0.75	0.81	0.83	0.88	0.91	0.74	0.77	0.81	0.86
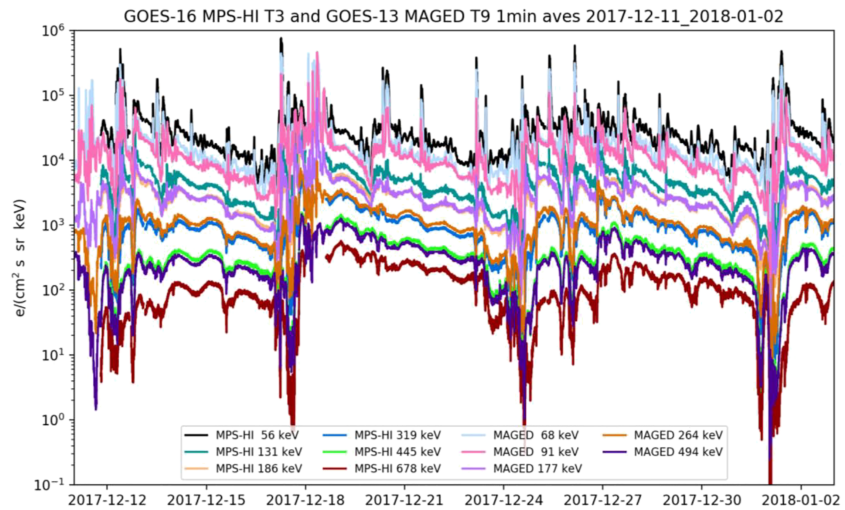
Figure 6. Flux time series for the near conjunction period from MPS-HI telescope 3 and MAGED telescope 9, both looking 70° north of the equatorial plane.

3.4. GOES-16 and GOES-17 Cross-Satellite Comparison

Finally, we compare the spectra of electron flux percentiles from the two GOES-R series satellites, GOES-16/-17. Figure 9 shows, in the same format, a comparison of the two telescopes 1 for the period 20 June 2018 to 24 September 2018, when both satellites were upright. During this period, GOES-17 was at 89.5°W and GOES-16 was at 75.2°W. For this plot, diamonds correspond to GOES-17 data and ×s denote the GOES-16 data. It is clear that the two distributions are very similar, with small discrepancies for a few low- to mid-energy channels. The comparisons for the five pairs of MPS-HI telescopes that look in the same direction are summarized in Table 8. The comparisons are made by taking the ratio of the GOES-16 to the GOES-17 percentile fluxes, following interpolation to 10 common energies (80, 130, 180, 278, 380, 550, 900, 1,493, 1,969, and 2,890 keV) assuming a piecewise power-law distribution. The sharp drops in the lower percentiles at the highest energies indicate that the reported fluxes are at residual background levels (the instrumental backgrounds having been subtracted from the measurements used in these comparisons).
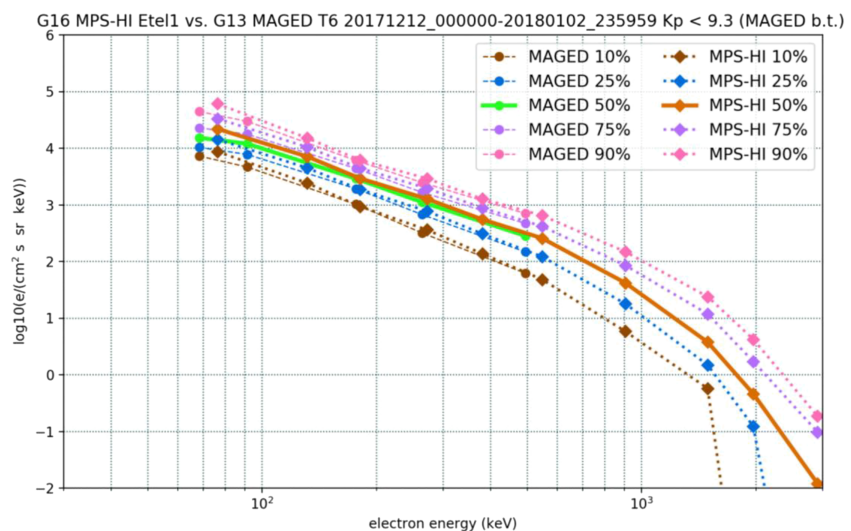

Figure 7. Comparison of GOES-16 MPS-HI telescope 1 and GOES-13 MAGED telescope 6 1-min percentile spectra. The period of comparison is 12 December 2017 to 2 January 2018 during near conjunction.

Table 6
Comparisons for the Five Pairs of GOES-13 MAGED and GOES-16 MPS-HI Telescopes That Look in the Same Direction During the Near-Conjunction Period. The Values are the Ratio of the GOES-13 to the GOES-16 Percentile Fluxes Interpolated at Five Energies

| E (keV)	MT9		Q :		ET3	MT6		Q :		ET1	MT1		Q :		ET4	MT8		Q :		ET2	MT7		Q :		ET5
	10	25	50	75	90	10	25	50	75	90	10	25	50	75	90	10	25	50	75	90	10	25	50	75	90
80	1.05	1.03	1.01	1.03	1.03	0.73	0.68	0.68	0.66	0.66	0.76	0.73	0.72	0.72	0.74	0.78	0.75	0.76	0.75	0.74	0.81	0.77	0.79	0.80	0.81
130	1.18	1.17	1.16	1.18	1.22	0.83	0.80	0.77	0.78	0.82	0.76	0.73	0.71	0.72	0.77	1.05	1.09	1.06	1.07	1.11	0.75	0.73	0.74	0.77	0.82
180	0.95	0.97	0.94	0.94	0.94	1.01	0.97	0.93	0.93	0.93	1.48	1.42	1.36	1.35	1.36	1.04	1.06	1.06	1.05	1.05	0.72	0.73	0.74	0.74	0.78
270	0.83	0.83	0.85	0.84	0.82	0.82	0.81	0.82	0.80	0.80	0.76	0.76	0.76	0.75	0.75	1.08	1.10	1.11	1.11	1.10	0.84	0.78	0.79	0.81	0.81
380	0.96	0.93	0.95	0.95	0.94	0.90	0.90	0.91	0.90	0.93	0.83	0.85	0.85	0.83	0.87	0.91	0.89	0.91	0.91	0.92	0.82	0.78	0.80	0.82	0.81
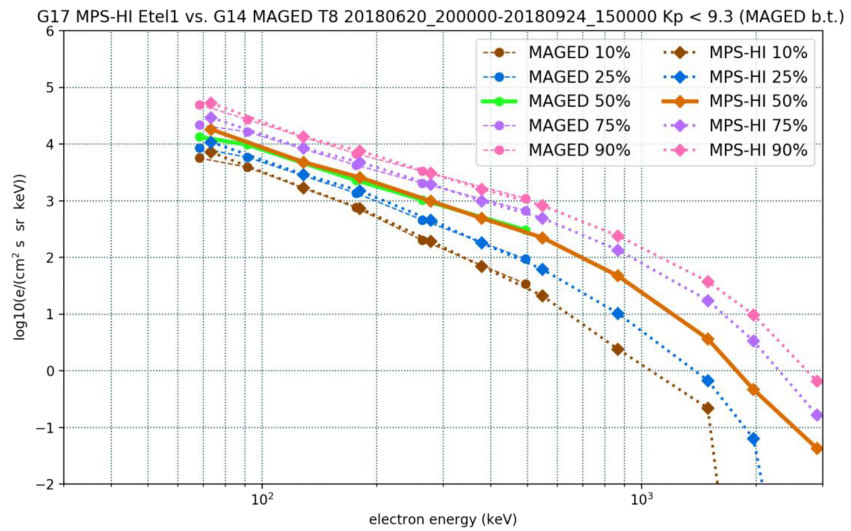
Figure 8. Comparison of GOES-17 MPS-HI telescope 1 and GOES-14 MAGED telescope 8 1-min percentile spectra. The period of comparison is 20 June 2018 to 24 September 2018.

3.5. Effect of MAGED Bowtie Characterization

In order to evaluate the effect of the bowtie characterization of MAGED, the root-mean-square (RMS) normalized median differences have been determined by subtracting from unity the median ratios in Tables 5–7 and calculating the RMS over all telescopes and energies. Similar comparisons (not shown) have been made of MPS-HI and MAGED fluxes with the latter attributed to the mean channel energies (see Table 3) and not adjusted for the bowtie geometrical factors. The RMS normalized median differences are summarized in Table 9. The results show that using the bowtie characteristics of the MAGED fluxes does result in better agreement overall with the MPS-HI fluxes. By comparison, a similar evaluation of Table 8 gives an RMS normalized median difference of 0.241.

3.6. Cross-Satellite Comparisons of >2-MeV Fluxes

The comparison of the GOES-13/-14 and GOES-16/-17 >2-MeV fluxes is less direct than at energies below 800 keV. While the GOES-16/-17 MeV fluxes come from the MPS-HI telescopes, on the earlier satellites, they are derived from measurements by the Energetic Proton, Electron and Alpha Detector (EPEAD) dome D3 detectors. The two EPEADs look eastward and westward (~100° full-width FOV) while the MPS-HI telescopes (30° full-width FOV) are arranged in a north-south fan centered on the radially outward direction. The geometrical factors for the EPEAD and MPS-HI >2-MeV channels are, respectively, 0.05 and 0.00076 $cm^2 \cdot sr$. Thus the >2-MeV comparisons involve detectors with different look directions and greatly different geometrical factors. Since the EPEAD FOVs usually encompass the pitch-angle range around 90° (unless the magnetic field is highly stretched), we compare their observations with MPS-HI telescopes 1 and 4, whose pitch angles are usually closest to 90°.

The integral fluxes (electrons/($cm^2 \cdot sr \cdot s$)) at the 50th, 75th, and 90th percentiles for the three comparison periods are tabulated in Table 10. The table is restricted to these percentiles since, during 2018, when the fluxes were less elevated, the 25% percentile of the MPS-HI observations lay within the residual noise of the background correction. The agreement is reasonable given the different detector characteristics and look directions. Agreement is best during the near-conjunction period. The EPEAD fluxes are substantially greater at the higher percentile levels. Possible reasons for these differences and their impact are discussed below.

4. Discussion

As a first comment, we need to discuss the fundamental limitation of the bowtie analysis: it only works when the bowtie technique training spectra are representative of the actual observed spectra in this region of space.

Table 7
Comparisons for the Five Pairs of GOES-14 MAGED and GOES-17 MPS-HI Telescopes That Look in the Same Direction. The Values are the Ratio of the GOES-14 to the GOES-17 Percentile Fluxes Interpolated at Five Energies

| E (keV)	MT7 : ET3					MT8 : ET1					MT1 : ET4					MT6 : ET2					MT9 : ET5				
	10	25	Q 50	75	90	10	25	Q 50	75	90	10	25	Q 50	75	90	10	25	Q 50	75	90	10	25	Q 50	75	90
80	0.68	0.66	0.65	0.65	0.68	0.80	0.78	0.76	0.77	0.83	0.70	0.68	0.67	0.67	0.73	0.58	0.57	0.57	0.57	0.59	0.57	0.54	0.55	0.53	0.54
130	0.82	0.79	0.80	0.81	0.86	0.99	0.95	0.96	0.96	0.98	0.88	0.83	0.85	0.86	0.87	0.75	0.73	0.75	0.77	0.78	0.73	0.71	0.70	0.70	0.69
180	0.81	0.80	0.80	0.79	0.80	0.96	0.86	0.85	0.85	0.85	1.04	0.95	0.97	0.94	0.96	0.76	0.75	0.75	0.75	0.76	0.67	0.63	0.62	0.61	0.60
270	0.85	0.85	0.91	0.93	0.95	0.88	0.88	0.94	0.95	0.98	0.98	0.97	1.04	1.05	1.07	0.82	0.83	0.87	0.88	0.91	0.77	0.74	0.79	0.78	0.73
380	0.80	0.79	0.83	0.86	0.87	1.04	1.02	1.04	1.08	1.09	1.03	1.01	1.03	1.09	1.09	0.91	0.84	0.88	0.94	0.93	0.94	0.85	0.86	0.86	0.82
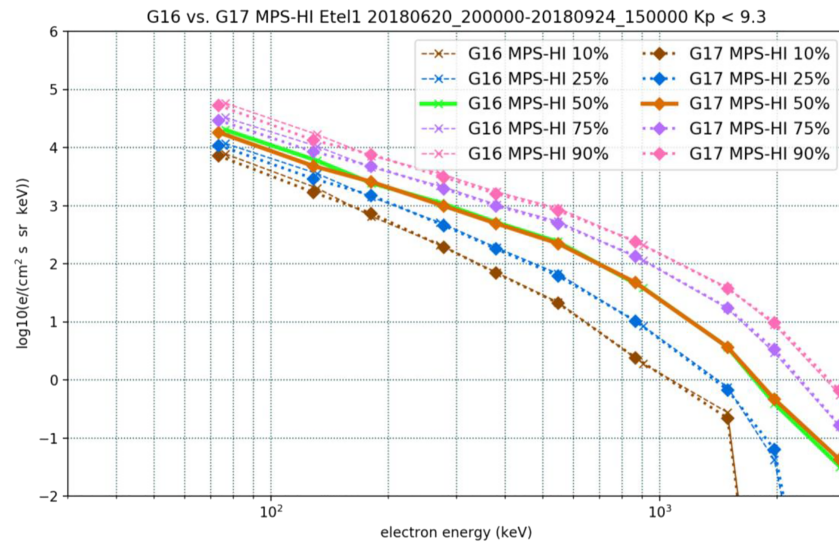
Figure 9. Comparison of GOES-16 and GOES-17 MPS-HI telescope 1 1-min percentile spectra. The period of comparison is 20 June 2018 to 24 September 2018.

At geostationary orbit, the typical spectrum is one of declining flux with energy. If the observed spectra, for example, happen to increase with energy, or have a high energy bump-on-tail, training of the bowtie analysis with the typical declining-flux-with-energy spectra will not give accurate results. Spectra that increase with energy and have a bump-on-tail are rare at geostationary orbit (Johnston et al., 2010). More importantly, the CRRES family of spectra we used to train the bowtie technique is an actual observed data set in the range $6 \leq L < 8$ and so any atypical spectra that are observed by GOES spacecraft are likely included in the CRRES training data set as well. We are therefore confident that the current bowtie analysis provides an accurate representation of the geostationary data observed by GOES.

Another issue with the bowtie analysis is the use of 1,000 random spectra to train the technique. In order to determine the dependency of the bowtie results on the random selection of training spectra, we ran the bowtie analysis 50 times with a different seed for the random number generator each time. We then calculated the standard deviation for each channel and each telescope, 55 in total. For GOES-16, the percent fractional variation of the effective energy/energy threshold ranges from 0.035% to 1.771%, while for the median GF, the same quantity ranges from 0.14% to 5.456%. For GOES-17, the percent fractional differences range from 0.019% to 1.423% and 0.289% to 5.555% for the effective energy/energy threshold and GF, respectively. We therefore believe that no significant error is introduced by using one run of the bowtie analysis with one seed for the random number generator of the 1,000 training spectra.

After the cross-satellite comparisons were presented in formal program reviews, the real-time processing of the GOES-16 and GOES-17 MPS-HI electron fluxes was approved to go forward using the bowtie *GdE* factors. To date, the MPS-HI electron fluxes from these two satellites have been processed using the bowtie *GdE* given above, and the current plan is to evaluate the *GdE* of future units similarly. The bowtie channel energies are reported in the MPS-HI data files. The comparisons described above demonstrate overall good agreement between the electron fluxes observed on GOES-13, -14, -16, and -17. Nonetheless, there are aspects of these comparisons that warrant a closer look.

The fluxes in GOES-16 MPS-HI telescope 4 channel E3 (181 keV) are unexpectedly low in comparison with both GOES-13 and GOES-17, as opposed to other channels and telescopes. A detailed reevaluation revealed no errors in the construction of E3's geometrical factor from the available data. In the future, it is probably best adjusted empirically using the rigorous telescope cross-calibration method of Rowland and Weigel (2012).

While E3 is not used at present for any real-time alerts, the differences between the responses of the GOES-13 and -14 and the GOES-16 and -17 >2-MeV channels to the radiation environment (Table 10)

Table 8
Comparisons for the Five Pairs of GOES-16 and GOES-17 MPS-HI Telescopes. The Values are the Ratio of the GOES-16 to the GOES-17 Percentile Fluxes

E (keV)	ET3 : Q					ET1 : Q					ET4 : Q					ET2 : Q					ET5 : Q				
	10	25	50	75	90	10	25	50	75	90	10	25	50	75	90	10	25	50	75	90	10	25	50	75	90
80	0.61	0.66	0.64	0.65	0.65	1.20	1.19	1.22	1.22	1.21	0.90	0.92	0.91	0.93	0.94	0.90	0.90	0.90	0.90	0.91	0.87	0.88	0.87	0.86	0.88
130	0.67	0.71	0.71	0.72	0.72	1.25	1.28	1.29	1.29	1.31	1.10	1.17	1.17	1.19	1.18	0.80	0.80	0.80	0.80	0.80	1.07	1.13	1.12	1.11	1.11
180	0.78	0.84	0.86	0.86	0.87	0.90	0.94	0.96	0.96	0.95	0.62	0.67	0.69	0.69	0.70	0.77	0.78	0.77	0.76	0.77	0.86	0.90	0.94	0.93	0.92
278	0.93	0.94	0.98	1.01	1.02	1.00	1.05	1.08	1.07	1.11	1.10	1.15	1.17	1.15	1.18	0.68	0.70	0.72	0.74	0.73	0.74	0.82	0.88	0.88	0.88
380	0.76	0.77	0.82	0.87	0.88	1.02	1.06	1.05	1.05	1.08	1.13	1.14	1.12	1.12	1.14	0.95	0.90	0.92	0.94	0.94	0.82	0.84	0.87	0.89	0.91
550	0.69	0.71	0.75	0.80	0.79	1.03	1.09	1.06	1.08	1.10	0.99	1.00	0.96	0.97	0.97	0.96	0.93	0.94	1.01	0.97	1.03	1.02	1.04	1.06	1.05
900	0.70	0.73	0.75	0.80	0.82	0.97	1.02	1.00	0.99	1.01	1.00	0.98	0.92	0.90	0.90	0.87	0.84	0.83	0.87	0.91	0.52	0.57	0.62	0.67	0.70
1493	1.17	0.93	0.65	0.69	0.78	1.25	1.11	1.00	0.97	1.03	0.69	0.67	0.68	0.67	0.68	1.58	1.14	0.98	1.02	1.13	1.00	0.93	0.73	0.69	0.76
1969	0.99	0.00	0.37	0.33	0.40	0.99	0.66	0.84	0.87	0.91	0.99	1.07	0.96	0.91	0.87	0.99	0.14	0.68	0.70	0.79	0.99	0.00	0.58	0.44	0.50
2890	1.00	0.96	0.52	0.67	0.37	1.00	1.16	0.77	0.96	0.86	1.00	1.17	0.81	1.02	1.13	1.00	1.13	1.06	0.86	0.46	1.00	0.96	0.36	0.71	0.60

Table 9
Normalized Median Differences of MAGED and MPS-HI Comparisons, With MAGED Characterized Using Bowtie Analysis Results and as Originally Processed

	GOES 13 vs. 16	GOES 13 vs. 16	GOES 14 vs. 17
	2017.01.09–2017.10.31	2017.12.12–2018.01.02	2018.06.20–2018.09.24
MAGED Bowtie	0.216	0.198	0.228
MAGED Original	0.242	0.287	0.262

will lead to systematic differences in the real-time alerts. The current plan is for the alerts to be based on the fluxes from the MPS-HI telescope 1 >2-MeV channel. Given the difference in the sensor types and look directions between the two satellite series, described above, some differences are to be expected. Even during the near-conjunction period, the GOES-16 >2-MeV channels registered systematically lower fluxes at the higher percentile levels than the GOES-13 channels (the alert level of 1,000 electrons/(cm2·sr·s) was near the 90th percentile during this period). The fact that the MPS-HI fluxes are lower may be due in part to differences between the energy responses of the EPEAD and MPS-HI >2-MeV channels, combined with the steepness of the energy spectra in this range. The MPS-HI >2-MeV channel response has a rather gradual turn on (Appendix A) with an effective lower energy of 2.075 MeV, while the EPEAD >2-MeV channel response has a sharp turn on at 2.00 MeV (Hanser, 2011). However, the observing geometry differences may be more important in explaining the discrepancies. The EPEAD Dome D3 integrates across a wide range of pitch angles (~90–100°) with a central pitch angle near 90°, while the MPS-HI telescopes 1 and 4 have much narrower FOVs whose central pitch angles tend to be offset from 90°. Therefore, the observed differences depend on the actual pitch-angle distributions, which vary with energy, *L*-shell, local time, and recent geomagnetic activity (Gannon et al., 2007). The effects of these observing geometry differences remain to be investigated quantitatively. Nonetheless, these comparisons indicate that the >2-MeV electron alerts based on MPS-HI observations will be issued slightly later than they were on GOES-15 and earlier satellites.

The bowtie effective energies of the lowest-energy MPS-HI and MAGED channels are high compared to the nominal band passes. This is a consequence of the high energy tails of the channel responses combined with the relatively flat spectra below 100 keV in the proxy data set used for the bowtie analysis. At the other end of the energy spectrum, the discrepancies between the GOES-16/-17 MPS-HI MeV electron channels are relatively large. The difficulties encountered with the proxy data set at these energies are described in Appendix B. In the future, the use of Van Allen Probes spectra (Boyd et al., 2019) to improve the bowtie proxy data set at low and high energies should be considered. However, care must be taken only to introduce spectral forms present at geostationary orbit, by using data from Van Allen Probes orbits that map to the vicinity of geostationary orbit, under select conditions generally on the nightside (Baker et al., 2019).

Although the spectral sampling by MPS-HI below 600 keV is only slightly improved over MAGED (six vs. five channels), the improvement in sampling between 600 keV and 2 MeV compared to EPEAD is substantial. In this important energy range for internal charging effects, EPEAD has a single integral channel, which is attributed to >0.8 MeV but whose actual response turns on gradually from 0.6 to 5 MeV (Hanser, 2011), making interpretation difficult. In contrast, MPS-HI has three differential channels with effective energies at ~900, 1,493, and 1,969 keV that define the spectrum in the range where its log-log slope steepens with increasing energy, as is evident in the percentile plots above. One benefit of the improved MPS-HI spectral sampling, combined with the effective energies from the bowtie analysis, is the ability to more easily calculate integral electron fluxes corresponding to actual shielding thicknesses, for example, by using the empirical electron range expressions of Tabata et al. (1972).

Table 10
Integral Fluxes of >2-MeV (electrons/(cm^2·sr·s)) at the 50th, 75th, and 90th Percentiles, for all Relevant Detectors (EPEAD/MPS-HI), and the Three Comparison Periods

Period	Detector	50%	75%	90%
20170109–20171031	G13 E	5.84E+02	3.36E+03	9.60E+03
	G13 W	6.63E+02	3.81E+03	1.04E+04
	G16 T1	4.89E+02	2.64E+03	7.83E+03
	G16 T4	5.91E+02	3.31E+03	8.05E+03
20171212–20180102	G13 E	1.14E+02	4.53E+02	1.21E+03
	G13 W	1.35E+02	5.26E+02	1.41E+03
	G16 T1	1.14E+02	3.26E+02	8.24E+02
	G16 T4	1.23E+02	3.97E+02	9.33E+02
20180620–20180924	G14 E	1.61E+02	1.43E+03	4.52E+03
	G14 W	1.47E+02	1.30E+03	4.20E+03
	G16 T1	1.23E+02	5.78E+02	2.19E+03
	G16 T4	1.25E+02	7.18E+02	2.50E+03
	G17 T1	1.26E+02	6.42E+02	2.33E+03
	G17 T4	1.47E+02	7.71E+02	2.78E+03

Table A1

Model/data selection for the response construction of the GOES-16 MPS-HI electron telescopes

GOES-16	ETel1	ETel2	ETel3	ETel4	ETel5
E1S	Gaussian + GEANT	Gaussian + GEANT	Gaussian + GEANT	Gaussian + GEANT	Gaussian + GEANT
E2	GEANT	GEANT	GEANT	GEANT	GEANT
E3t	Data + GEANT	Data + GEANT	Data + GEANT	Data + GEANT	Data + GEANT
E4	GEANT	GEANT	Data + GEANT	GEANT	Data + GEANT
E5	GEANT	GEANT	Data + GEANT	GEANT	Data + GEANT
E6	GEANT	GEANT	Data + GEANT	GEANT	Data + GEANT
E7	Data + GEANT	GEANT	Data + GEANT	GEANT	Data + GEANT
E8	GEANT	GEANT	GEANT	GEANT	GEANT
E9	GEANT	GEANT	GEANT	GEANT	GEANT
E10	GEANT	GEANT	GEANT	GEANT	GEANT
E11	GEANT	GEANT	GEANT	GEANT	GEANT

5. Conclusions

In the present study, we demonstrated the use of the bowtie inversion technique for the characterization of the GOES SEISS MPS-HI electron channels and its application in the calibration of the GOES spacecraft energetic electron data. The introduction of the bowtie analysis has simplified the application of the broad spectral responses of the MPS-HI electron channels in the data processing. Cross-satellite comparisons of the 1-min averaged electron spectra have demonstrated good agreement between the various GOES spacecraft data sets. The results establish the bowtie inversion technique as a valid method for deriving a simple processing algorithm for MPS-HI.

Appendix A: Instrument Responses

There are two sources of information for the channel geometric factors: (1) the GEANT4 simulations given the channel specifications and (2) measurements of the channel responses at specific energies conducted at various high energy electron beam facilities. The former provides a continuous variation of the GFs with energy (even though based on theoretical principles), while the latter provides direct measurements of the responses (albeit at only a few discreet energies). Details of the response acquisition from these methods are beyond the scope of this paper.

For our purposes, we used a combination of model and data for the channel responses. The mix of model and data was channel and telescope dependent, and it involved considerations of main peak energy shifts between model and data, anomalous/missing data points, overall model scaling with data, and long high energy tails that were not always directly measured. In general, the model response was selected (appropriately scaled in magnitude to match the data) whenever the two were in good agreement in terms of the energy edges of the main peak. If the measurements exhibited a peak shifted with respect to the model, then the data response was selected. In this case, a model tail was added beyond the highest measured energy up to 10 MeV. In cases of missing/anomalous data points, model points were added to suitably fill the gaps/replace the data, respectively. The final selections for all telescopes and channels are shown in Tables A1 and A2 for GOES-16 and GOES-17, respectively.

The final choice of model/data mix was fitted with B splines (Dierckx, 1993). The motivation for fitting the geometrical factors is to provide a smoothly varying tabular function at high energy resolution for the purposes of numerical integration. Simple linear interpolation does not provide a realistic solution, although it may give a low error solution if points are close together. B splines are used as smoothing splines rather than interpolations. Therefore, noise in the measured results will tend to be smoothed out. A B spline is a one-dimensional smoothing

Table A2

Model/data selection for the response construction of the GOES-17 MPS-HI electron telescopes

| GOES-17	ETel1	ETel2	ETel3	ETel4	ETel5
E1S	Data + GEANT	Data + GEANT	Data + GEANT	Data + GEANT	Data + GEANT
E2	Data + GEANT	Data + GEANT	Data + GEANT	Data + GEANT	Data + GEANT
E3t	GEANT	GEANT	GEANT	GEANT	GEANT
E4	GEANT	GEANT	GEANT	GEANT	GEANT
E5	GEANT	GEANT	GEANT	GEANT	GEANT
E6	GEANT	GEANT	GEANT	GEANT	GEANT
E7	GEANT	GEANT	GEANT	GEANT	GEANT
E8	GEANT	GEANT	GEANT	GEANT	GEANT
E9	GEANT	GEANT	GEANT	GEANT	GEANT
E10	GEANT	GEANT	GEANT	GEANT	GEANT
E11	GEANT	GEANT	GEANT	GEANT	GEANT
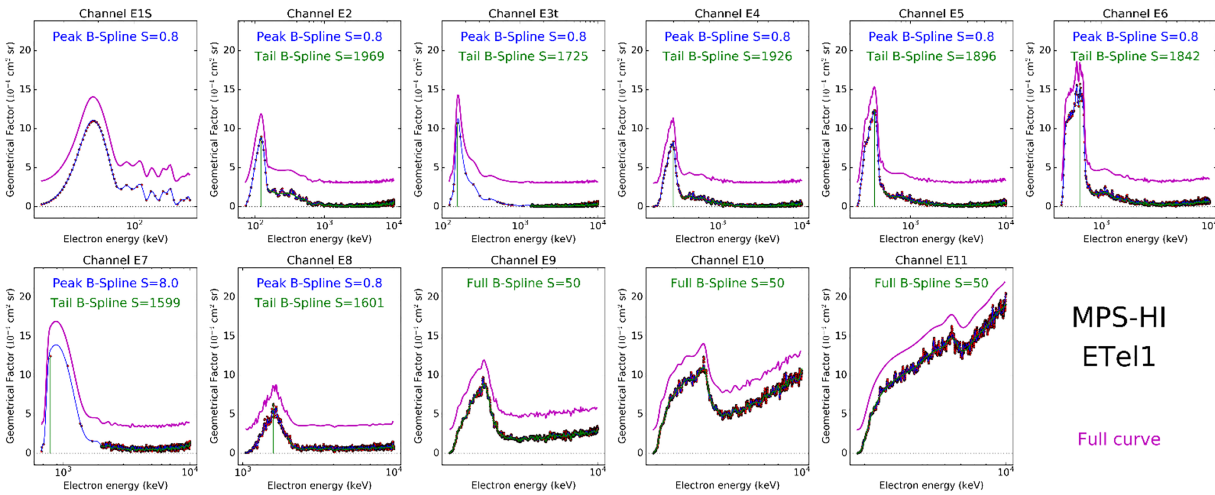
Figure A1. Application of the B-spline fitting for GOES-16 SEISS MPS-HI telescope 1. Each panel corresponds to an electron channel, as marked at the top. Depending on the channel, one or two fits of the model and/or data points were performed, as denoted above the curves. The blue curves are a low S fit (near-interpolation fit), appropriate for the response main peak, where more precision is needed. The green curves are a high S fit (near-polynomial fit) more appropriate for the highly variable tail, or the entire curve for channels E9-E11, where more smoothing is needed. The pink curves are the merging of the two fits (or the single fit for channels E1S and E9–E11), shifted upwards for clarity.
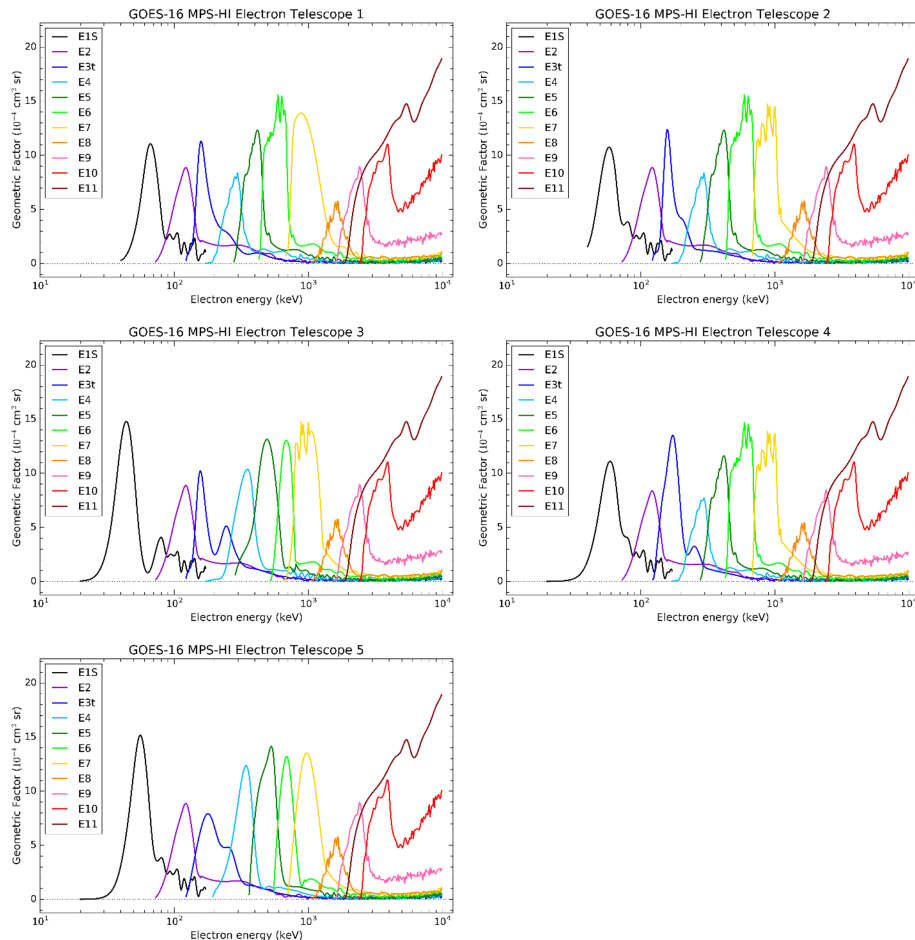
Figure A2. Results of the B-spline fitting for the responses of the GOES-16 MPS-HI electron telescopes. Each panel corresponds to an electron telescope, with different channels color coded according to the legend.
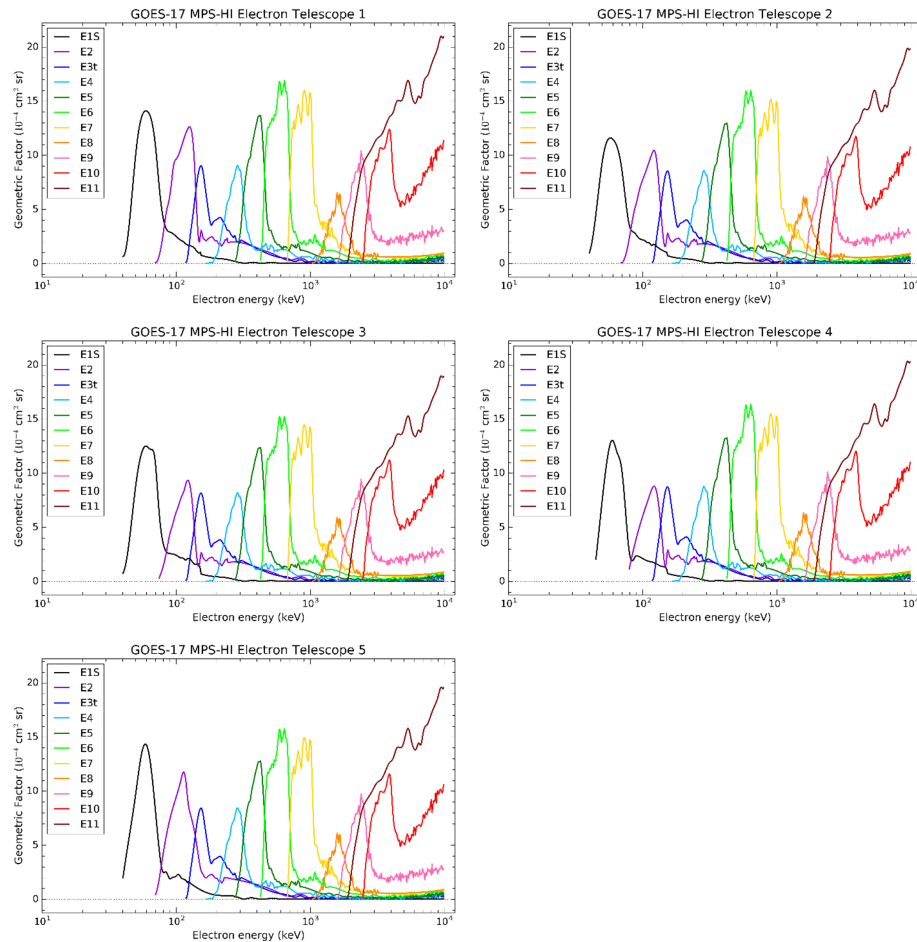
Figure A3. Results of the B-spline fitting for the responses of the GOES-17 MPS-HI electron telescopes. Each panel corresponds to an electron telescope, with different channels color coded according to the legend.

spline fit to a set of data points. The user-specified smoothing factor S is used for an interchange between an interpolating spline (that passes over all data points) and a least squares polynomial fit (that smooths the existing data); this single parameter "... controls the tradeoff between closeness of fit and smoothness of fit" (Dierckx, 1993). In the extreme cases, the function will return an interpolating spline if $S = 0$ and a weighted least squares polynomial if S is very large (the degree of the polynomial can be specified by the user, with cubic spline being used here).

Figure A1 demonstrates the application of the B-spline fitting technique for the GOES-16 SEISS MPS-HI telescope 1. Similar fits were performed for the remaining telescopes. Each panel corresponds to an electron channel as marked at the top. Depending on the channel, one or two spline fits of the model and/or data were performed, as denoted above the curves. The blue curves are a low S fit (near-interpolating spline fit), appropriate for the response main peak, where more precision is needed. The green curves are a high S fit (least squares polynomial fit), more appropriate for the highly variable tail, or the entire curve for channels E9–E11, where more smoothing is needed. The pink curves are the merging of the two fits (or the single fit for channels E1S and E9–E11), shifted upwards for clarity. For the GOES-16 telescopes (as the one shown here), a Gaussian fit of the E1S measurements was chosen, instead of the original data, to which a short GEANT4 tail was added (not up to 10 MeV as for the other channels). This was not done for the GOES-17 telescopes for which the original beam measurements were utilized, plus a long tail up to 10 MeV. For channels E2–E8, the tail fit S value was set to a fraction of the model points present. For channels E9–E11, the entire curve was originally fit with a low S value but subsequently fit with a high $S = 50$ value for a more smooth representation. Figures A2 and A3 illustrate the resulting electron responses for GOES-16 and GOES-17, respectively.
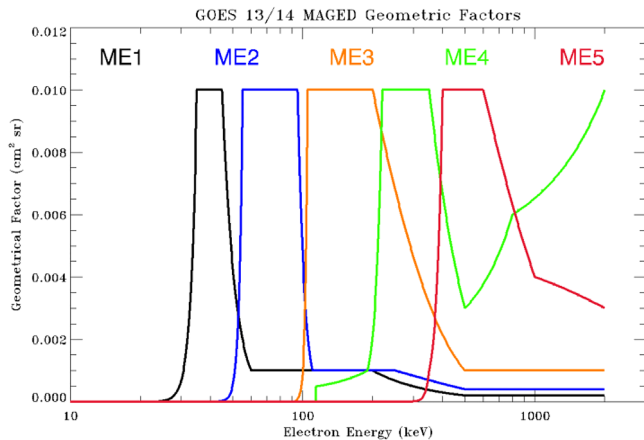
Figure A4. GOES-13/−14 MAGED responses.

For comparison and completeness, Figure A4 shows the GOES-13/-14 MAGED responses. In addition, the energy response of the EPEAD >2-MeV electron channel is given by Hanser (2011), tables 6–37.

Appendix B: HEEF Data Fit

The HEEF spectra, of the combined MEA/HEEF proxy CRRES dataset, are extrapolated to 10 MeV using either an exponential or a power-law approximation. The choice of the extrapolating function depends on the presence and quality of the data. The process consists of the following steps:

1. Check for the presence or not of HEEF data. At least five data points ≥ 1.6 MeV should be present.
2. If at least five HEEF data points are present, check on the quality of the fit with a power-law function. This is judged to be good when the fit $\chi^2 < 0.2$.
3. If the above two conditions are met, use the present HEEF data, with a power-law extrapolation (based on the present HEEF data) for missing points up to 10 MeV.
4. If not, then use exponential fit (Selesnick & Blake, 2000) based on the existing MEA/HEEF data.

The process is illustrated in Figure B1. All four panels show energy spectra, flux versus energy. The two panels on the left are for an event with good quality HEEF data on 29 March 1991, 084630.1 UT, and the two panels on the right are for an event with low quality HEEF data on the same day but at 083030.1 UT. The two bottom panels show the MEA (orange) and HEEF (blue) data separately, with light green marking the test power-law fit of the existing HEEF data. The top two panels show the MEA/HEEF data (dark green), the power-law fit of the HEEF data (light green), and the final selection for the MEA/HEEF proxy data (red), including the extrapolations. The thin vertical orange dashed lines in all panels mark the extent of the MEA data, the thin vertical blue dashed lines mark the extent of the HEEF data, and the thicker vertical blue dashed line (near 3 MeV) marks the 5th HEEF data point ≥ 1.6 MeV.

In the case on the left, more than five HEEF data points are present (first requirement), and the power-law fit $\chi^2 < 0.2$ (second requirement); therefore, the present HEEF data are used and extrapolated to 10 MeV with a
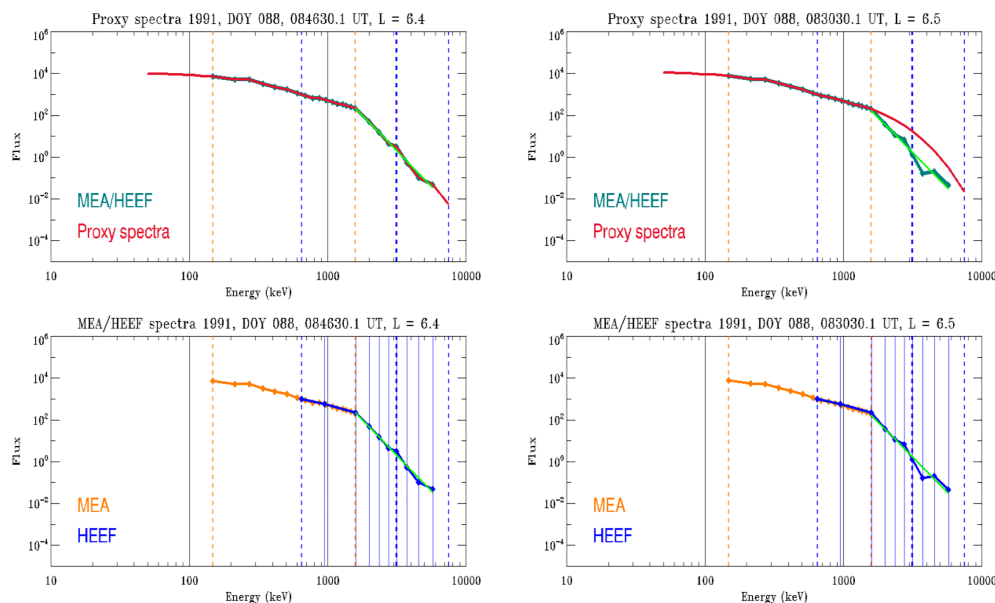

Figure B1. Application of the HEEF data extrapolation: (left) power-law extrapolation and (right) exponential extrapolation. For both left and right panels, the bottom panel shows the MEA (orange), and HEEF (blue) data, with the power-law fit in light green. The top panels show the MEA/HEEF data (dark green), the power-law test fit (light green), and the eventual selection for the proxy data set (red).

power law of the same slope as the fit. In the case on the right, more than five HEEF data points are present, but the power-law fit $\chi^2 > 0.2$. In this case, the exponential extrapolation of the entire HEEF range above 1.6 MeV is used. The same exponential extrapolation applies also when there are fewer than five HEEF data points present.

The inclusion of a switch between exponential extrapolation of missing or low-quality high energy HEEF data, and the use of the original data plus a power-law extrapolation to 10 MeV, improves the errors of reproducing the original CRRES fluxes from the inversion of the count rates given by equation 1, as discussed at the end of section 2. This is particularly evident for the high energy MPS-HI channels E8-E10 during periods of high magnetospheric activity when the high energy portion of the HEEF spectrum is present.

References

Baker, D. N., Zhao, H., Li, X., Kanekal, S. G., Jaynes, A. N., Kress, B. T., et al. (2019). Comparison of Van Allen Probes energetic electron data with corresponding GOES-15 measurements: 2012–2018. *Journal of Geophysical Research: Space Physics*, *124*(12), 9924–9942. https://doi.org/10.1029/2019JA027331

Boyd, A. J., Reeves, G. D., Spence, H. E., Funsten, H. O., Larsen, B. A., Skoug, R. M., et al. (2019). RBSP-ECT combined spin-averaged electron flux data product. *Journal of Geophysical Research: Space Physics*, *124*(11), 9124–9136. https://doi.org/10.1029/2019JA026733

Dichter, B. K., Galica, G. E., McGarity, J. O., Tsui, S., Golightly, M. J., Lopate, C., & Connell, J. J. (2015). Specification design and calibration of the space weather suite of instruments on the NOAA GOES-R program spacecraft. *IEEE Transactions on Nuclear Science*, *62*(6), 2776–2783. https://doi.org/10.1109/TNS.2015.2477997

Dierckx, P. (1993). *Curve and surface fitting with splines*. Oxford, United Kingdom: Oxford Univ. Press.

Fillius, R. W., & McIlwain, C. E. (1974). Measurements of the Jovian radiation belts. *Journal of Geophysical Research*, *79*(25), 3589–3599.

Gannon, J. L., Li, X., & Heynderickx, D. (2007). Pitch angle distribution analysis of radiation belt electrons based on Combined Release and Radiation Effects Satellite Medium Electrons A data. *Journal of Geophysical Research*, *112*(A5), A05212. https://doi.org/10.1029/2005JA011565

Grubb, R. N. (1975). *The SMS/GOES Space Environment Monitor Subsystem (NOAA Technical Memorandum ERL SEL-42)*. Boulder, Colo: Space Environment Laboratory.

Hanser, F. A. (2011). *EPS/HEPAD calibration and data handbook (Tech. Rep. GOESN-ENG-048D)*. Carlisle, Mass: Assurance Technology Corporation. [Available at. http://www.ngdc.noaa.gov/stp/satellite/goes/documentation.html

Johnston, W. R., Lindstrom, C. D., & Ginet, G. P. (2010). Characterization of radiation belt electron energy spectra from CRRES observations. In *AGU Fall Meeting Abstracts,* SM33C-1925.

Johnston, W. R., Lindstrom, C. D., & Ginet, G. P. (2014). *CRRES Medium Electron Sensor A (MEA) and High Energy Electron Fluxmeter (HEEF): Cross-calibrated data set description (Technical Report AFRL-RV-PS-TR-2014-0016)*. Kirtland AFB, NM: Air Force Research Laboratory.

Meredith, N. P., Horne, R. B., Isles, J. D., & Rodriguez, J. V. (2015). Extreme relativistic electron fluxes at geosynchronous orbit: Analysis of GOES E > 2 MeV electrons. *Space Weather*, *13*(3), 170–184. https://doi.org/10.1002/2014SW001143

Nagai, T. (1982). Local time dependence of electron flux changes during substorms derived from multi-satellite observation at synchronous orbit. *Journal of Geophysical Research*, *87*(A5), 3456–3468. https://doi.org/10.1029/JA087iA05p03456

NASA (2011). *Mitigating in-space charging effects–A guideline (NASA Technical Handbook NASA-HDBK-4002A)*. Washington, DC: National Aeronautics and Space Administration.

Nelder, J. A., & Mead, R. (1965). A simplex method for function minimization. *The Computer Journal*, *7*(4), 308–313.

Onsager, T. G., Chan, A. A., Fei, Y., Elkington, S. R., Green, J. C., & Singer, H. J. (2004). The radial gradient of relativistic electrons at geosynchronous orbit. *Journal of Geophysical Research*, *109*(A5), A05221. https://doi.org/10.1029/2003JA010368

Onsager, T. G., Grubb, R., Kunches, J., Matheson, L., Speich, D., Zwickl, R., & Sauer, H. (1996). Operational uses of the GOES energetic particle detectors. In E. R. Washwell (Ed.), *GOES-8 and beyond*, *Proc. SPIE* (Vol. 2812, pp. 281–290). Bellingham, Wash: Int. Soc. for Opt. Eng.

Panametrics (2004). Electron calibration report, GOES NO/PQ MAGED telescope. GOESN-ENG-028. [Available at https://ngdc.noaa.gov/stp/satellite/goes/documentation.html]

Rowland, W., & Weigel, R. S. (2012). Intracalibration of particle detectors on a three-axis stabilized geostationary platform. *Space Weather*, *10*(11), S11002. https://doi.org/10.1029/2012SW000816

Sandberg, I., Aminalragia-Giamini, S., Provatas, G., Hands, A., Ryden, K., Heynderickx, D., et al. (2019). Data exploitation of new Galileo environmental monitoring units. *IEEE Transactions on Nuclear Science*, *66*(7), 1761–1769. https://doi.org/10.1109/TNS.2019.2915686

Selesnick, R. S., & Blake, J. B. (2000). On the source location of radiation belt relativistic electrons. *Journal of Geophysical Research*, *105*(A2), 2607–2624.

Tabata, T., Ito, R., & Okabe, S. (1972). Generalized semiempirical equations for the extrapolated range of electrons. *Nuclear Instruments and Methods*, *103*(1), 85–91.

Vampola, A. L. (1987). Thick dielectric charging on high-altitude spacecraft. *Journal of Electrostatics*, *20*(1), 21–30.

Van Allen, J. A., Baker, D. N., Randall, B. A., & Sentman, D. D. (1974). The magnetosphere of Jupiter as observed with Pioneer 10, 1. Instrument and principal findings. *Journal of Geophysical Research*, *79*(25), 3559–3577.

Wrenn, G. L. (1995). Conclusive evidence for internal dielectric charging anomalies on geosynchronous communications spacecraft. *Journal of Spacecraft and Rockets*, *32*(3), 514–520.

Wrenn, G. L., & Smith, R. J. K. (1996). Probability factors governing ESD effects in geosynchronous orbit. *IEEE Transactions on Nuclear Science*, *43*(6), 2783–2789.